MVV super Coster–Kronig spectra of nickel near the excitation threshold

2005 J. Phys.: Condens. Matter 17 7029

(http://iopscience.iop.org/0953-8984/17/43/020)

INSTITUTE OF PHYSICS PUBLISHING JOURNAL OF PHYSICS: CONDENSED MATTER

J. Phys.: Condens. Matter **17** (2005) 7029–7052 doi:10.1088/0953-8984/17/43/020

MVV super Coster–Kronig spectra of nickel near the excitation threshold

P Songsiriritthigul[1,2], W Wongkokua[1,2,4], H Nakajima[1], W Pairsuwan[1,2], T Ishii[1,2] and A Kakizaki[3]

[1] National Synchrotron Research Center, 111 University Avenue, Muang District, Nakhon Ratchasima 30000, Thailand
[2] School of Physics, Suranaree University of Technology, 111 University Avenue, Muang District, Nakhon Ratchasima 30000, Thailand
[3] Institute for Solid State Physics, University of Tokyo, Kashiwa, Chiba 277-8581, Japan

E-mail: hiden@nsrc.or.th

Received 12 May 2005, in final form 16 September 2005
Published 14 October 2005
Online at stacks.iop.org/JPhysCM/17/7029

Abstract

The MVV super Coster–Kronig (sCK) spectra of metallic Ni have been measured near the 3p excitation threshold by varying excitation photon energy. The results have been interpreted on the basis of the Cini–Sawatzky theory. The measured sCK band has composite structure with features at electron kinetic energy of 49.8, 56.3, 59.5, and 60.5 eV. If we interpret the band at 49.8 eV to be the split-off quasi-atomic band, we can estimate the effective intra-atomic Coulomb energy at a large value of 8 eV. The spectral shape of the MVV sCK band measured by excitation with vacuum ultraviolet light does not coincide with that obtained by the Mg Kα excitation or with that of the L_3VV Coster–Kronig band. The shape of the MVV sCK spectrum changes as excitation energy changes. The excitation-energy range in which such spectral change occurs extends from the 3p threshold to 10 eV above it. As the kinetic energy for the MVV sCK band starts to overlap that of the two-hole-bound-state band, the MVV sCK band changes its shape considerably and the two spectra become inseparable. In this excitation-energy region, the spectator electron excited optically forms a virtual bound state with the two 3d holes. The location of the apparent two-hole-bound-state band shifts toward high binding energy on the 3p–3d resonance. This can be interpreted as a kind of final state interaction. The suggested intermediate and final states of the single-step transition are consistent with the constant-initial-state spectra and total photoyield spectrum. The roles of the screening by conduction electrons and the sd hybridization are emphasized.

[4] On leave from: Department of Physics, Faculty of Science, Kasetsart University, Bangkok 10900, Thailand.

1. Introduction

The electronic structure of transition metals is quite interesting, since localized and itinerant aspects coexist there. Particularly, the valence shell photoemission of metallic Ni shows distinctive aspects originating from the correlation involving a 3d hole existing in the ground state. The relevant phenomena are the generation of the two-hole bound state and the associated p–d resonance excitation [1]. The p–d resonance corresponds to the radiationless resonant Raman scattering in the atomic transition. A lot of work has been carried out on the two-hole bound state. Up to the present, pertinent scientists have agreed upon the electronic structure and the generation mechanism of the two-hole bound state [2–5].

The p–d resonance involving the two-hole bound state takes place because the two-hole bound state as the final state of the direct transition can also be reached by indirect Auger transitions such as the Coster–Kronig (CK) or super Coster–Kronig (sCK) effect following the optical excitation of the core electron. In this report, we deal with the MMM sCK transition of Ni in relation to the 3p–3d resonance; hereafter, MMM is designated MVV, where V stands for the valence band. The MVV sCK spectra of metallic Ni have *not* been investigated well. We have found only one report by Björneholm *et al* [6] so far. The optical excitation of a 4s electron, a conduction electron, is not taken into account in the present study, since it is weak and gives only a broad background feature.

A great deal of research work has been reported on the Auger effect. When a hole is generated in a deep core level, the several different Auger transitions occur in the cascade mode. In some cases, the optical excitation of the core electron and the Auger transition do not occur in the two-step process but in the one-step process. If the excited electron is brought to a low lying unoccupied level, the Auger process may be equivalent to the Raman process accompanying the emission of an electron. This process is referred to as the radiationless resonant Raman scattering. Armen *et al* [7] reported a detailed review on the Auger transitions of rare gases. Fundamental physical processes regarding the resonant Auger effects are described in this article with abundant experimental data.

The Auger effect is a phenomenon occurring in the inner-shell levels of an atom and related transitions are seemingly localized to the atom. In solids, particularly in metals and alloys, however, the phenomena are not so simple, since valence–conduction electrons involved in the processes are itinerant. Kleiman [8] reviewed the physical processes governing the Auger transitions caused by the optical excitation of electrons in deep core levels in metals. The central interest is in the question whether the Auger spectra are quasi-atomic or band-like. By the influence of the strong potential of a core hole, the outer-shell electrons are attracted to the core and the system becomes atomic-like. This state is referred to as quasi-atomic. Kleiman [8] selected d-band metals with high correlation and nearly-free-electron metals like alkali metals as examples. In the articles, the issues of the general many-body interaction, the quasi-atomic model, and the screening effects are described. Theoretically calculated binding energies are compared with those of experimental data. Another interesting problem is the emergence of satellites.

Physically interesting examples are found in 4d transition metals. Siervo *et al* [9] analysed the $M_{4,5}VV$ spectra of Rh, Pd and Ag caused by the excitation of the L_3 electron and subsequent generation of two holes in the $M_{4,5}$ state. They concluded that the process in Rh is band-like and those in Pd and Ag are quasi-atomic. The shake-up satellites accompanying the $M_{4,5}VV$ spectrum were found. This is a characteristic aspect showing the transfer from the adiabatic regime to the sudden regime. Grehk *et al* [10] observed the excitation energy dependence of the $L_3M_{4,5}M_{4,5}$ CK transition and the $L_3N_{4,5}N_{4,5}(L_3VV)$ CK transition across the L_3 edge on Pd. They found the Fano type resonance features. Drude *et al* [11] analysed the excitation

energy dependence of the $L_3M_{4,5}M_{4,5}$ ($^1G_4$) spectrum of Ag near the excitation edge. Thus, they did not observe the transition from the adiabatic to sudden approximation regimes. The adiabatic transition regime corresponds to photoelectrons of low energy which tend to screen the core hole. This affects the lineshape in the way that the Auger satellites of Ag disappear in the adiabatic regime [12]. In the case of 4d transition metals, the initial hole is created in the deep core level and the hole is transferred to the outer core levels. The physical interest is in the screening of the holes by the outer-shell electrons.

A lot of reports have been published on the Auger effects of 3d transition metals as well [13–18]. Data are on the line shape analyses of the LVV CK spectra [13, 14, 17] and Cu MVV sCK spectra [15]. Kivimäki *et al* [18] measured the excitation energy dependence of the $M_3M_{4,5}M_{4,5}$ sCK spectrum of Ge and separated the resonant sCK transition coexisting with the normal sCK transition. Himpsel *et al* [16] analysed the line shape of the $M_3M_{4,5}M_{4,5}$ sCK spectrum of Zn using the Doniach–Šunjić theory [19] and concluded the transfer from the adiabatic regime to the sudden regime occurs. Föhlisch *et al* [20] and Coulthard *et al* [21] showed that the line shape of the LVV CK spectrum of Cu consists of atomic multiplet components (^1G, ^1D, ^1S, ^3F, ^3P).

The aspects of the MVV sCK spectra of metallic Ni are contrasted to the case of atomic Ni on which some reports [22, 23] have appeared. The reported data on atomic Ni are different from those of metallic Ni. Schmidt *et al* [22] measured the MVV sCK spectra of some transition metal atoms by excitation with electron beams. Their MVV sCK spectra of atomic Ni are different from corresponding spectra of metallic Ni by Björneholm *et al* [6] and from those presented in this report [24]. The MVV sCK spectra of atomic Ni excited with synchrotron radiation soft x-rays were reported by Tiedtke *et al* [23]. These spectra are quite different from the spectrum obtained by excitation with electron beams [22]. They are also different from those of metallic Ni. In this report, we refer to metallic Ni as Ni unless otherwise stated.

In the final state of the emission of electrons from the 3d band, two configurations are possible. In one configuration only one 3d hole exists, and in the other configuration two 3d holes appear. When a 3d electron is ejected from the 3d band, conduction electrons screen the remaining two holes instantaneously. It is possible through this process that a hole is removed by recombination with a conduction electron and only a hole is left in the 3d band as

$$V(h) + h\nu \rightarrow V(h+h) + \mathrm{e_p} \tag{1}$$

$$V(h+h) + \mathrm{e} \rightarrow V^*(h). \tag{2}$$

Here, $h\nu$ is photon energy. $V(h)$ represents the 3d band with a hole at the Fermi level, $V^*(h)$ the 3d band with an excited hole, and $V(h+h)$ the 3d band with two holes. $\mathrm{e_p}$ is the ejected photoelectron and e a screening conduction electron. Practically, the hybridization occurs between the pure 3d and 4s (conduction) states [3, 4].

In the final state of photoemission, where the screening by conduction electrons is insufficient, the two-hole bound state occurs as

$$V(h+h) + \mathrm{e} \rightarrow V(h^2) + \mathrm{e}^*. \tag{3}$$

Here, $V(h^2)$ represents the two-hole bound state and e^* is an electron trapped (bound weakly) by the two bound holes.

The two-hole bound state does not show dispersion. This is proved experimentally [6, 25–28]. Thus, the two-hole bound state has often been treated as a quasi-atomic state with the electronic configuration of $3d^8 4s$. The two-hole bound state has two characteristics: One is that it gives rise to the spin polarization of emitted photoelectrons [29, 30]. This offers direct evidence of the generation of the two-hole bound state.

The second is resonance [3–6, 27]. In a certain excitation-energy region, the two-hole bound state is formed by the excitation of a 3p or 2p electron. By the excitation of a p core

electron near the excitation threshold, the filled-up 3d state is generated and it becomes the intermediate state for the MVV sCK or LMM (LVV) CK transition leading to the two-hole bound state as

$$V(0) + p(h) \rightarrow [V(h^2) + e^*] + e_A. \tag{4}$$

Here, $p(h)$ represents the core hole, $V(0)$ the filled 3d band, and e_A the Auger electron. The final state involving the two-hole bound state produced directly through the transition expressed by equation (3) cannot be distinguished from that produced through the sCK or CK transition as equation (4) if the optical excitation energy is almost the same as the Auger electron energy. Therefore, the transitions through the two channels resonate and interfere with each other [3–5]. The resulting excitation spectrum has the profile characteristic of the resonance and interference.

The theoretical work known as the Cini [31] and Sawatzky [32] theory treats the Auger transition involving the energy band in metals with 3d electrons. The theory starts with a filled valence band and considers the final state with two holes. The Auger spectrum is obtained by calculating the pertinent Green's function. The Cini–Sawatzky theory [31, 32] states the following nature of the spectrum: the Auger spectrum is given by the energy band scheme and has the shape of the self-convolution of the density-of-states (DOS) curve of the filled energy band, if the width of the valence band, W, is much larger than the intra-atomic Coulomb energy, U ($W \gg U$). In case of $W \ll U$, the spectrum is quasi-atomic and the line spectrum appears. In the intermediate region, the quasi-atomic and band spectra coexist.

The self-convoluted band is considerably deformed depending on the magnitude of W/U. Sawatzky and Lenselink [32] and Bennett *et al* [33] carried out a model calculation using the Cini–Sawatzky theory [31, 32] with the DOS curve of a rectangular shape and showed how the Auger spectrum changes its shape according to the magnitude of W/U. Bennett *et al* [33] measured the LVV CK spectra of Ni and its alloys and compared the results with those of their calculation. No sharp line spectrum was found in their observed results, but they analysed the composite profile of their spectra in terms of multiplet lines of the final state electronic configuration of d^8. In the case of Ni, in which the 3d band is not filled up, the final state with two holes is reached if the complete screening by conduction electrons takes place.

As mentioned above, plenty of reports have been published so far on the LVV CK spectra of Ni [34–44]. This tendency has been continuing up to now. The reported work covers experimental [33–35], theoretical [36, 37], resonance [38–41], spin-resolved [38], and coincidence [42–44] studies. Experiments at low temperature will come out in the near future [45].

The recent tendency [20, 21, 46] is that investigations of the LVV CK spectra are carried out more on Cu than on Ni. In Cu, the 3d band is filled up and located further below the Fermi level as compared with that of Ni. Even if satellites accompany the main 3d band, the ambiguity in the analysis is reduced. Because of this, detailed experiments are carried out.

2. Experimental details

A sample used is a slice cut from a single crystal of Ni(111) bought from Goodfellow Cambridge. The purity of the crystal is 99.999%. The slice was polished by an ordinary procedure. By measuring x-ray Laue patterns, we confirmed the sample surface has the orientation of (111).

The sample surface was cleaned with alcohol and pure water in an ultrasonic bath. The sample surface was further cleaned *in situ* in vacuum of 10^{-10} mbar. The final cleaning of the sample was made by the repetition of Ar ion bombardment followed by heating by electron

bombardment. The temperature of the sample was monitored with a thermocouple fixed to the sample holder and a pyrometer to measure the surface temperature. The temperature indication of both monitors was different: when the sample holder temperature was 1030 K, the sample surface temperature was 900 K. By the Auger analyses, the existence of foreign atoms or molecules on the sample surface such as O, S, and CO was examined. Cycles of Ar ion bombardment and heating were repeated for a month before a clean surface was obtained. The well defined (111) surface was confirmed by measuring the low-energy electron diffraction pattern.

Photoemission measurements were performed at BL4 of the Siam Photon Source of the National Synchrotron Research Center of Thailand. The details of the beam line were reported elsewhere [47]. Light from a bending magnet part of a 1 GeV storage ring was used. The light beam is focused onto the entrance slit of a monochromator with a toroidal mirror. The monochromator is of a vertical dispersion type and equipped with plane gratings of non-linear groove spacing. By using three gratings with average groove spacings of 300, 600, and 1200 lines mm^{-1}, optical measurements can be carried out over the range from $h\nu = 20$ to 240 eV. An intermediate slit and a focusing mirror are installed between the incident slit and the grating. A rear mirror focuses monochromatized light to a small spot on the sample surface.

Angle-integrated energy distribution curves (EDCs) of photoelectrons and Auger electrons were measured with a Thermo VG Scientific CLAM2 energy analyser. For angle-resolved EDC measurements, a hemispherical analyser of a different type is also installed in the analyser chamber.

A He discharge tube and an x-ray tube are installed in the analyser chamber as additional light sources. The performance of the energy analyser was measured with the He I line (21.2 eV). The spectra in the x-ray photoemission spectroscopy (XPS) were also measured to obtain complementary data. The resolution of the energy analyser was estimated at 220 meV from the measurement of the Fermi edge of Au at room temperature by excitation with the He I line. This is the energy resolution of our system for the MVV sCK measurements. Since the intensity of excitation light was not high, we were not able to make the slit width narrow. The overall resolution in the photoemission measurements was 620 meV at $h\nu = 60$ eV.

Measurements of photoemission were carried out at room temperature with light incident on the sample surface at normal incidence. The electric vector of light was parallel to the sample surface. The surface condition was frequently examined and the surface was cleaned by Ar ion bombardment and subsequent heating, if it was degraded. The pressure in the measurement chamber was in the 10^{-11} mbar range and a clean surface lasted for about 8 h.

3. Results

Figure 1 shows the photoemission spectrum of the valence-band region of Ni(111) and the concomitant MVV sCK spectrum. The abscissa represents the kinetic energy of emitted electrons and the ordinate the electron intensity. EDC was measured with light at $h\nu = 79$ eV. At this excitation energy, the Fermi edge occurs at 74.2 eV in photoelectron kinetic energy, ε_k. The peak of the two-hole-bound-state band is at $\varepsilon_k = 67.9$ eV. This energy of the peak position is equivalent to the binding energy, ε_b, of 6.3 eV. The spectrum shown in figure 1 coincides with those in reported data of the valence shell photoemission of Ni. The MVV sCK band extends from $\varepsilon_k = 48.5$ to 63.5 eV. The band width is 15 eV. As is obvious in figure 1, the distinctive aspect of the MVV sCK is that it is very broad and the intensity is low.

We consider that there are three kinds of two-hole states. One is the state of two bare holes. The two holes remain at a lattice site for a very short time; one of the 3d holes may be

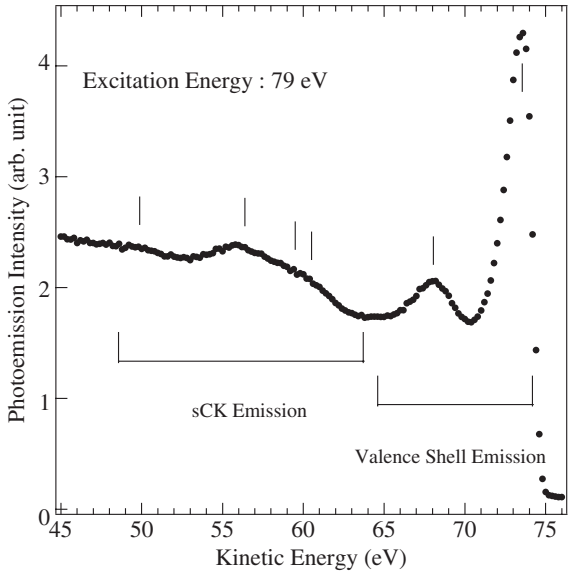

Figure 1. Photoelectron EDC of Ni(111) measured in the angle-integrated mode. The abscissa represents the kinetic energy of photoelectrons and the ordinate their intensity. The energy of excitation light is 79 eV. Vertical bars indicate major features in the spectrum. EDC exhibits both MVV sCK and valence band spectra, as marked in the figure.

extinguished by combining with a conduction electron. The second is the state of two holes weakly screened by the conduction electron generated optically. In this report, this state is referred to as the quasi-two-hole-bound state. The third is the two-hole bound state. The three possible two-hole states are schematically illustrated in figure 2. The bare two-hole state designated as $V(h+h)$ is illustrated in figure 2(a). In figure 2(b), two 3d holes screened weakly by an electron generated by the optical excitation of a 3p electron are illustrated. In figure 2(c), the two-hole bound state is illustrated. White circles represent 3d holes and black dots the screening electrons. Arrows emphasize that the electrons are emitted from the crystal. The intermediate state giving rise to the MVV sCK transition will be explained later.

We will conclude that the MVV sCK spectrum changes its profile as excitation photon energy approaches the 3p excitation threshold; the shape of the MVV sCK band varies in a way that it cannot be distinguished from the two-hole-bound-state band. Thus we have to observe and find the profile of the sCK band definitely with excitation light with energy sufficiently high as compared to the threshold energy.

Figure 3 shows the results of the measurements of the profile of the MVV sCK band. The spectrum shown in figure 3 is the average of seven EDCs measured at excitation energy from $h\nu = 80$ to 110 eV at an interval of 5 eV. The full line is a smoothed curve at six adjacent measured points. The abscissa represents the kinetic energy and the ordinate the photoelectron intensity. The background is subtracted. Vertical bars in the figure indicate the locations of apparent features in EDC. They occur at $\varepsilon_k = 49.8$, 56.3, 59.5, and 60.5 eV. The locations were determined with some ambiguity and thus the values below the decimal point are not accurate. The locations of the features at $\varepsilon_k = 59.5$ and 60.5 eV are confirmed by means of the second-derivative spectra. An arrow indicates the location of the high-energy limit of the MVV sCK band. It is located at $\varepsilon_k = 63.5$ eV.

The spectrum shown in figure 3 is broad and no well defined feature is resolved except one at $\varepsilon_k = 49.8$ eV. This weak feature forms a single resolved band with a half width of

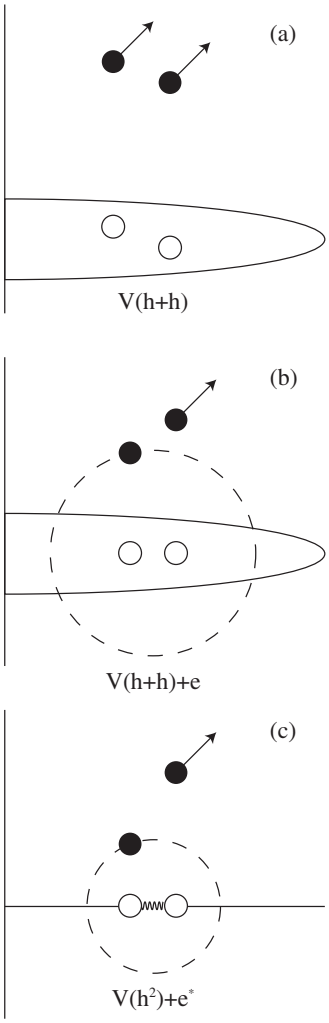

Figure 2. Three possible final states of the MVV sCK transition of metallic Ni. White circles represents holes in the 3d bands. Black dots are electrons. Arrows emphasize that the electrons are emitted from the crystal. $V(h+h)$: the state of two bare holes in the valence shell. $V(h+h)+$e: the state where two holes are weakly screened by an optically excited electron. $V(h^2)+$e*: two-hole bound state.

1.7 eV. If the instrumental resolution is taken into account, it has a width of 1.6 eV. It has been reported that the 3p core hole state has a value of spin–orbit splitting of 1.8 eV [49]. However, the spectrum in figure 3 does not show it. In the photoemission spectrum of the 3p core level of Ni, several split lines are found [6]. They are attributed to the multiplet lines due to the exchange interaction between the photoproduced 3p hole and 3d electrons. In the 3p spectra of isolated Ni atoms excited with synchrotron radiation in the vacuum ultraviolet light region, the number of observed multiplet components is much larger because of the mixing of many different configurations [23]. This appears to indicate that the j–j coupling scheme to form the spin–orbit split levels in the final state of the transition is not dominant. In contrast, in the MVV sCK spectrum of atomic Ni excited with the electron beam [22] only a single line is found and its composite structure is not clear.

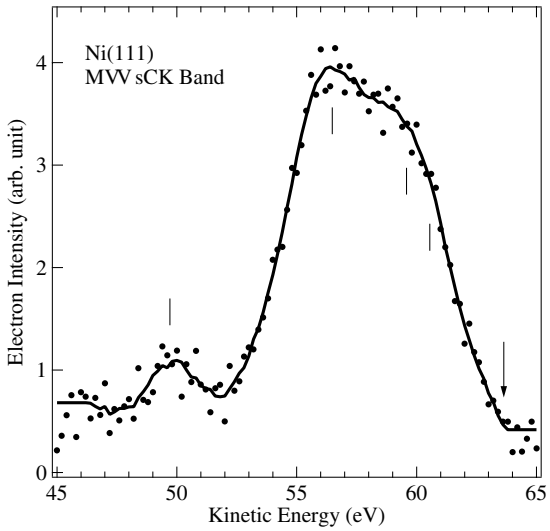

Figure 3. EDC of the MVV sCK electron. The abscissa represents the kinetic energy of emitted electrons and the ordinate their intensity. The spectrum is obtained by averaging seven EDCs measured at excitation energy from 80 to 110 eV at an interval of 5 eV. The solid line indicates the smoothed curve obtained by the six-point average. Vertical bars at 49.8, 56.3, 59.5, and 60.5 eV indicate major features of EDC. An arrow at 63.5 eV indicates the high-energy limit of the MVV sCK band.

We measured the XPS spectrum of the emission of 3p electrons. The result agrees qualitatively with that reported by Björneholm *et al* [6]. The values of the binding energy of features in EDC observed in the present work are slightly different from those of Björneholm *et al* [6] and two lines found in the present work are missing in their spectrum. The XPS 3p lines are explainable in terms of the multiplets formed by the electronic configuration of $3p^5 3d^9$. The lifetime of this final state is very short and the 3d hole is destroyed through screening by conduction electrons.

In figure 4, the MVV sCK band presented in figure 3 is compared with that measured with Mg Kα radiation. At the top of the figure, the smoothed spectrum illustrated in figure 3 is indicated. At the middle, EDC measured with Mg Kα radiation is shown. For reference, the L_3VV CK spectrum measured by Mårtensson *et al* [35] is also shown at the bottom in the figure. The L_3VV CK spectrum is placed so that the main peak at $\varepsilon_k = 846.2$ eV aligns to the main peak of the MVV sCK spectrum. Later, Weinelt *et al* [40] measured the L_3VV CK spectrum using synchrotron radiation. The L_3VV CK spectrum shown in figure 4 almost coincides with that measured with light at $h\nu = 1082.3$ eV. It also coincides with that measured by Bennett *et al* [33].

Three EDCs shown in figure 4 do not coincide rigorously with each other. In the case of the L_3VV CK spectrum, the number of features is different from that of MVV sCK band measured with light in the region from 80 to 110 eV. The number of features of the MVV sCK spectrum measured with light at $h\nu = 80$–110 eV seems to be different from that of the MVV sCK spectrum measured by excitation with Mg Kα radiation. In the XPS spectrum, a weak shoulder feature is found at $\varepsilon_k = 57.5$ eV which is not found in EDC averaged over the region of excitation energy $h\nu = 80$–110 eV. The relative intensities of components of the MVV sCK spectrum measured with excitation light at $h\nu = 80$–110 eV are different from those measured by excitation with Mg Kα radiation. The spectrum measured with Mg Kα radiation

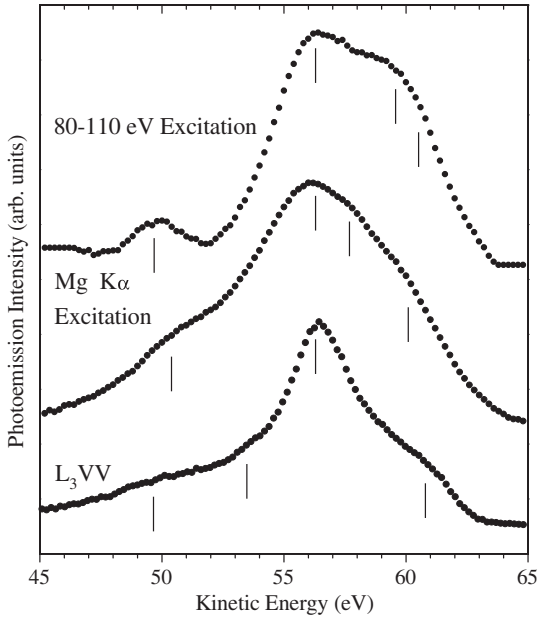

Figure 4. The MVV sCK spectrum exhibited in figure 3 (top) as compared with the MVV sCK spectrum obtained by excitation with Mg Kα radiation (middle). The abscissa represents the kinetic energy of emitted electrons. The L_3VV CK spectrum from [35] (bottom) is also shown for comparison. The L_3VV CK spectrum is placed in the figure so that the major peak is aligned to those of other two spectra. Features in each spectrum are indicated with vertical bars. The backgrounds are subtracted.

is not well resolved. Particularly, the component at $\varepsilon_k = 49.8$ eV is not well separated in the spectrum measured with Mg Kα radiation.

The profile of the MVV sCK spectrum is clearly different from that of the L_3VV CK spectrum; not only the number and relative locations of the component features but their relative heights are different. In particular, the intensity ratio of the highest intensity peak assigned to the ^{1}G level to the highest-kinetic-energy peak, ^{3}F, of the L_3VV CK spectrum does not coincide with the similar ratio in the MVV sCK spectrum. In the L_3VV CK spectrum, the lowest-kinetic-energy peak, ^{1}S, has the shoulder profile. In the MVV sCK spectrum, the similar feature has a relatively low intensity. These items of disagreement are not ascribable to the final states of the transitions, since the apparent final states are the same in both spectra. The results described so far seem to indicate that the spectral profiles of the MVV sCK and L_3VV CK spectra are not only determined by the valence states in the final states but the intermediate state with optically generated core holes and excited spectator electrons.

Björneholm *et al* [6] interpreted the apparent deformation of the MVV sCK spectrum on resonance as being caused by an overlapping satellite band at $\varepsilon_b = 13.5$ eV. In order to obtain more information on this issue, EDCs on the high-binding-energy side of the two-hole-bound-state band were measured in the excitation-energy region below the threshold of the 3p core excitation. Weak satellites observed by Okane *et al* [27] were also found here. In EDCs measured at $h\nu = 67$ and 68 eV, a weak feature is found around $\varepsilon_b = 13.5$ eV. Such weak satellites are conspicuous only on resonance. This point will be discussed later regarding the features in the second-derivative curves.

The excitation spectrum of the two-hole-bound-state band presents quite important information on the consideration of the cause of the deformation of the MVV sCK band.

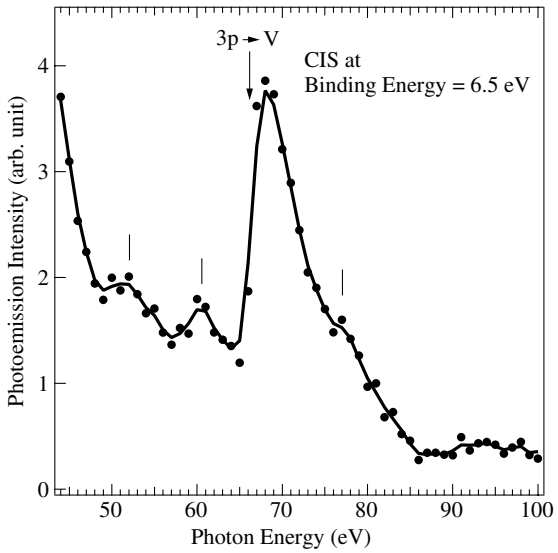

Figure 5. The CIS spectrum for photoelectrons with binding energy of 6.5 eV. The abscissa represents the excitation photon energy. The ordinate represents the photoelectron intensity at binding energy of 6.5 eV. Weak peaks at 52, 60.5, and 77 eV are indicated by vertical bars. The main resonance band has its peak at 68 eV and the onset position is recognized as a dip at 64 eV. The 3p excitation threshold is assigned to occur at 66.2 eV and exhibited with an arrow.

Here we give it in the form of the constant-initial-state (CIS) spectrum. Figure 5 shows the CIS spectrum in which the photoemission intensity at $\varepsilon_b = 6.5$ eV normalized to the incident photon intensity is plotted versus excitation photon energy. In the figure, weak features are indicated with vertical bars. They occur at $h\nu = 52$, 60.5, and 77 eV. We assign the location of the 3p threshold to be at $h\nu = 66.2$ eV and indicate it with an arrow in figure 5. This value coincides with the reported value of the binding energy of the M_3 ($3p_{3/2}$) level [49]. Just below the threshold of the 3p excitation, a dip occurs. It is located at $h\nu = 65$ eV. Increase in the photoemission intensity is noticed below $h\nu = 49$ eV. Its origin is unknown at present. One possibility of the origin is the decrease of the absorption cross section toward high photon energy according to the $(h\nu)^{-7/2}$ dependence in the region far above the threshold. In addition to this, the existence of the Cooper minimum [50] enhances the tendency of the decrease. The CIS spectrum illustrated in figure 5 coincides with the reported excitation spectrum of the 3p–3d resonance [27]. The origins of a broad band around $h\nu = 52$ eV and a peak at $h\nu = 60$ eV are not known at present. The origin of a shoulder feature around $h\nu = 77$ eV is not known, either. It should be remarked in figure 5 that the resonance band is broad. The resonance band has a peak at $h\nu = 68$ eV and a full width at half maximum (FWHM) of 5.2 eV. If we consider that the resonance band extends from $h\nu = 64$ to 85 eV, the resonance-energy region covers an area of width 21 eV. The result described above is contrasted to the resonant inverse photoemission data [51], which indicate the width of the empty 3d band enhanced resonantly to be about 1 eV. The width of the 2p–3d resonance band is also narrow, about 1 eV.

In order to see the change in the profile of the MVV sCK band more clearly, we show EDCs for $79 \geqslant h\nu \geqslant 71$ eV in figure 6. The abscissa represents the electron kinetic energy. Excitation energy is indicated on the left side of each EDC. Vertical bars indicate the locations of pertinent features in the spectra. Arrows at $\varepsilon_k = 63.5$ eV indicate the location of the high-energy limit of the MVV sCK band as shown in figure 3. As is distinct in EDCs for $h\nu = 77$

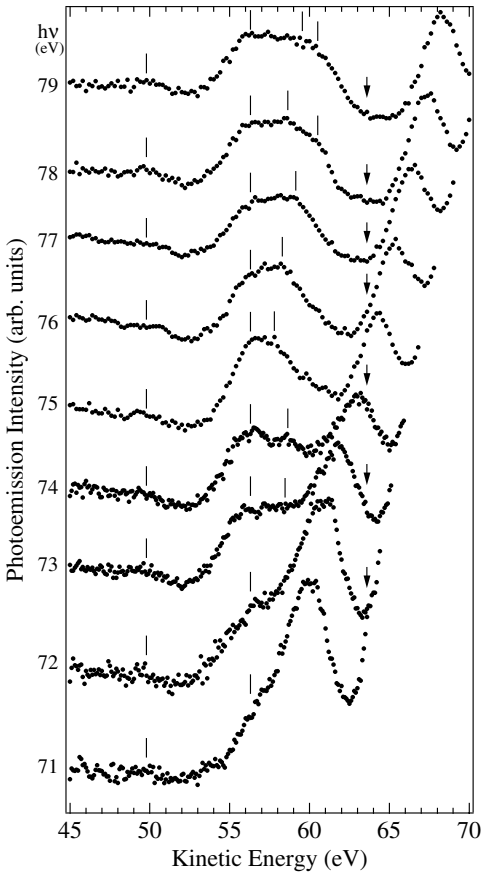

Figure 6. The MVV sCK and two-hole-bound-state spectra in the excitation-photon-energy range from 71 to 79 eV. The abscissa represents the kinetic energies of emitted electrons. The excitation photon energy for each EDC is exhibited on the left side of the figure. Vertical bars indicate the locations of the features at 49.8, 56.3, 59.5, 60.5 eV and those of a few features occurring in the area between 57 and 59.5 eV. Arrows show the locations of the high-energy limit of the MVV sCK band given in figure 3.

and 78 eV, the profile of the MVV sCK band is deformed even for the excitation energy for which the two-hole-bound-state band does not overlap the MVV sCK band. For $h\nu \leqslant 76$ eV, the two-hole-bound-state band overlaps the MVV sCK band. The MVV sCK band is deformed considerably and the feature at $\varepsilon_k = 59.5$ eV disappears. EDCs in the excitation-energy region, $h\nu \leqslant 76$ eV, do not seem to consist of overlapping independent bands that are the two-hole-bound-state band and the MVV sCK band, although the peak around $\varepsilon_b = 6.3$ eV remains distinctly. The original profile of the MVV sCK band is completely dissolved there. In other words, the MVV sCK band and the two-hole-bound-state band mix with each other to form a new band with a complicated profile.

The complete merger of the two spectra occurs at excitation photon energy of $h\nu = 68$ eV. It is interesting to investigate the situation described above from the two-hole-bound-state band side. In figure 7, EDCs for the generation of the two-hole bound state in the excitation-energy region $71 \geqslant h\nu \geqslant 66$ eV are illustrated. In this case, the abscissa represents the binding energy. The excitation photon energy is indicated on the left side of each EDC. The width,

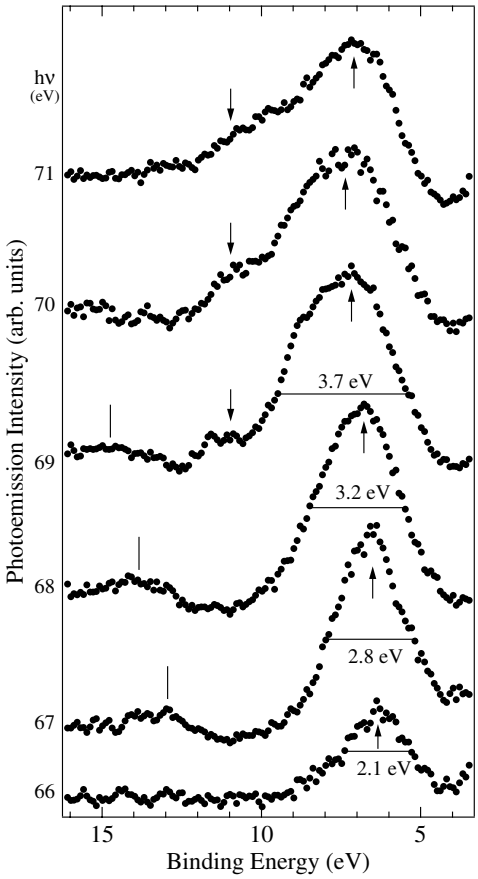

Figure 7. The two-hole-bound-state spectra in the excitation-energy range from 66 to 71 eV. The abscissa represents the binding energy. The excitation photon energy for each EDC is exhibited on the left side of the figure. Upward arrows indicate the peak positions. Downward arrows indicate the locations of the 11 eV satellite. Vertical bars exhibit the locations of the weak component of the MVV sCK band occurring at kinetic energy of 49.8 eV. The numbers given under the two-hole-bound-state bands are the values of the full widths at half maximum of the bands indicated with horizontal bars. The backgrounds are subtracted.

FWHM, of the pertinent emission band is indicated under each EDC with a horizontal bar. Downward arrows indicate the location of the 11 eV satellite. In EDC for $h\nu = 71$ eV, it is not clear whether or not the feature shown by the downward arrow is the 11 eV satellite. It may also be a part of the MVV sCK band. Regarding the locations of the 11 eV satellite in EDCs for $h\nu = 69$ and 70 eV, we cannot exclude the possibility that a feature ascribable to an origin other than the satellite occurs at this binding energy by accidental coincidence. Suppose it is the satellite, then it should be found at any excitation energy. However, it emerges only on resonance. Regarding the satellite at 13.5 eV, it cannot be separated clearly in figure 7. A feature is found around 13.5 eV in EDCs for $h\nu = 67$ and 68 eV, although the MVV sCK peak at $\varepsilon_k = 49.8$ eV occurs there as indicated with vertical bars.

The distinctive aspect of figure 7 is that the width of the two-hole-bound-state band is enhanced as the excitation energy is increased and the band shape is changed to be asymmetric and deformed. The peak position which is indicated with an upward arrow is also shifted

slightly toward high binding energy. In EDCs for $h\nu = 70$ and 71 eV, the existence of the 11 eV feature makes the asymmetry of the band profile more enhanced. However, the 11 eV feature cannot be separated from the two-hole-bound-state band clearly. Even in EDCs for $h\nu = 66$ and 67 eV, the band width increases in spite of the fact that the band asymmetry is not quite conspicuous. EDC for $h\nu = 69$ eV has a width larger than that of EDC for $h\nu = 66$ eV by about 76%. In EDC for $h\nu = 71$ eV, the width reaches 2.8 times as large as that for $h\nu = 66$ eV. The conclusion drawn from the observation given in figure 7 is that the two-hole bound state is also changed. The simple two-hole bound state is lost here.

In order to recognize the shift of the locations of features clearly, we take the second derivative of EDC. The second derivative deletes the part of the spectrum where the intensity changes slowly and makes the features emerge as definite peaks. Since the second derivative of a band has the negative sign in the band maximum area, we use the negative value of the second derivative. In figure 8, we plot the locations of the peaks in the second derivative curves versus excitation photon energy. The abscissa represents the kinetic energy of emitted electrons and the ordinate excitation energy. The black bands represent the widths and heights of features. The horizontal width of the band represents the width of a feature in the second derivative curve and the vertical width the peak height. The relation of the width of the band and the peak height is shown in the upper part of the figure. The locations of the peaks of the features are indicated with white dots. The locations of the peaks of the main 3d bands and the two-hole-bound-state band are shown by connecting measured points with straight lines. The lines represent the relation $\Delta\varepsilon_k = \Delta h\nu$ (constant-binding-energy lines). In the photon-energy region, $74 \geqslant h\nu \geqslant 67$ eV, the locations of the peaks of the two-hole-bound-state bands deviate from the constant-binding-energy line. The deviation occurs toward low kinetic energy. As is obvious from figure 5, the 3p–3d resonance occurs in this photon-energy region. In the LVV CK case, the locations of the two-hole-bound-state peaks deviate from the constant-kinetic-energy line toward the high kinetic energy on resonance [40]. The deviation of the peak position was also reported by Sakisaka *et al* [26]. We will interpret the deviation of the peak position from the constant-binding-energy line as being caused by the final state interaction.

Vertical lines in figure 8 exhibit the locations of features at $\varepsilon_k = 49.8$, 56.3, 59.5, and 60.5 eV of the MVV sCK band as shown in figure 3. The broken line indicates the high-kinetic-energy limit of the MVV sCK band at $\varepsilon_k = 63.5$ eV. In the areas where the MVV sCK band cannot be separated from the two-hole-bound-state band, the areas are shown with hatches connecting both bands. It is noticed that the peak position of the second derivative of the apparent two-hole-bound-state band deviates from the constant-binding-energy line in the excitation-energy region where the MVV sCK band cannot be clearly separated from the two-hole-bound-state band (resonance region) as pointed out already.

The peak around $\varepsilon_k = 56.3$ eV of the MVV sCK band aligns along the line of the constant kinetic energy of 56.3 eV. On the other hand, the feature around $\varepsilon_k = 59.5$ eV does not align well on the pertinent constant-kinetic-energy line except for EDCs obtained with high-energy photons. This is partly because the location of the shoulder feature cannot be assigned uniquely. The appearance of a definite peak in the second derivative curve at the shoulder feature of original EDC cannot necessarily be expected.

In figure 8, four constant-binding-energy lines are depicted. They are for $\varepsilon_\mathrm{b} = 0.6$ eV, the main 3d band, $\varepsilon_\mathrm{b} = 6.3$ eV, the two-hole-bound-state band, $\varepsilon_\mathrm{b} = 11$ eV, a satellite, and $\varepsilon_\mathrm{b} = 13.5$ eV, a satellite. Some measured peak positions align on these straight lines. It was pointed out that the satellite transition occurring at $\varepsilon_\mathrm{b} = 13.5$ eV may resonate with the MVV sCK transition and change the apparent profile of the MVV sCK spectrum on resonance [6, 24]. However, the satellite at $\varepsilon_\mathrm{b} = 13.5$ eV cannot be recognized unless the MVV sCK

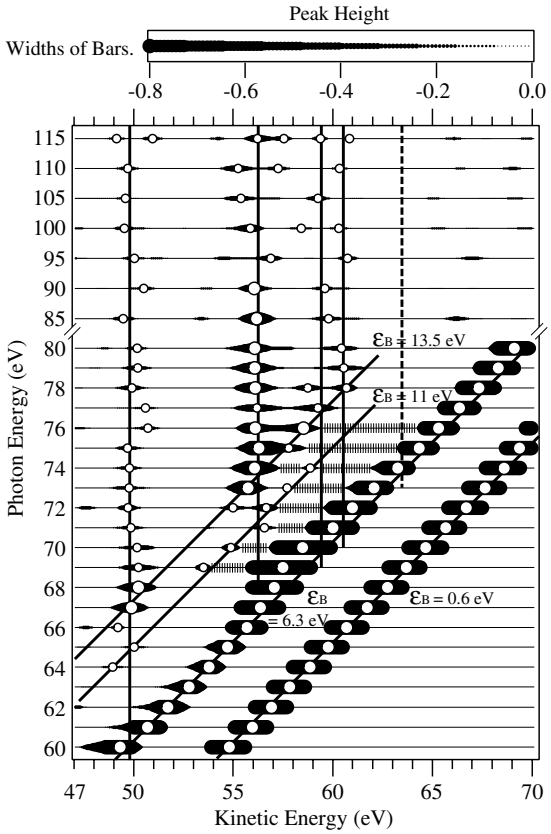

Figure 8. The relation between the excitation photon energy and the peak positions of features in the spectra of the second derivative of EDC. The abscissa represents the kinetic energy of emitted electrons and the ordinate the excitation photon energy. White dots indicate the locations of the peaks (negative sign). Black horizontal bands exhibit features and their locations occurring in the second derivative spectra. The widths of the horizontal bands indicate the depths of the negative peaks. The relation between the width of the band and the depth of the peak is illustrated above the figure. In the excitation-energy region from $h\nu = 69$ to 76 eV, the areas where the continuous bands exist is shown by hatches. Constant-binding-energy lines, given as $\Delta\varepsilon_k = \Delta h\nu$ ($\varepsilon_k + \varepsilon_b + \chi = h\nu$; χ is the work function), for $\varepsilon_b = 0.6$, 6.3, 11, and 13.5 eV are depicted. Full vertical lines exhibit the locations of the features of the MVV sCK band at $\varepsilon_k = 49.8$, 56.3, 59.5, and 60.5 eV shown in figure 3. The broken vertical line exhibits the location of the high-energy limit of the MVV sCK band at $\varepsilon_k = 63.5$ eV.

band occurs around $\varepsilon_b = 13.5$ eV as is distinct from figure 8. Thus, we do not treat the satellite at $\varepsilon_b = 13.5$ eV seriously as the cause of the spectral profile change.

In figure 8, a peak is evident at $\varepsilon_k = 49.8$ eV. Figure 7 shows that the corresponding peak indicated with vertical bars is resonantly enhanced over the excitation-energy range from $h\nu = 67$ to 69 eV. In this excitation-energy range, other components of the MVV sCK band merge into the two-hole-bound-state band completely. The component line at $\varepsilon_k = 49.8$ eV disappears for excitation energy below $h\nu \leqslant 66$ eV. This is because the threshold of the 3p excitation is at $h\nu = 66.2$ eV and the 3p hole is not generated for photon energy below $h\nu = 66$ eV. This means that the MVV sCK transition does not occur below $h\nu = 66$ eV.

Figure 9 shows the total yield spectrum. The abscissa represents the excitation photon energy and the ordinate the photocurrent flowing out of the specimen. The ordinate intensity

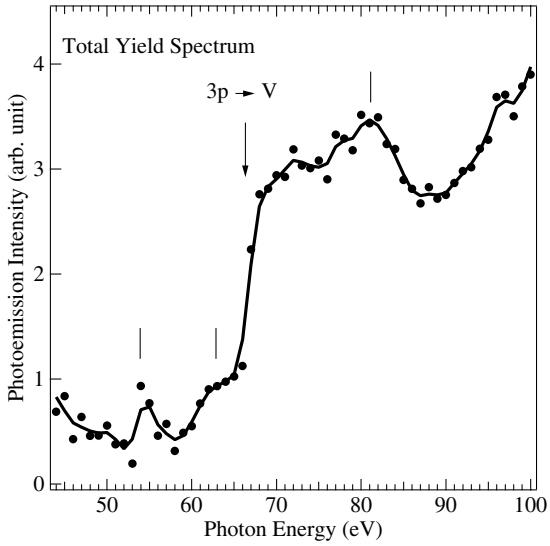

Figure 9. The total photoelectron yield spectrum. The abscissa represents the excitation photon energy and the ordinate the photocurrent flowing out of the specimen. Vertical bars indicate the locations of weak features at 54, 63, and 81 eV. The location of the threshold of the 3p excitation is shown by an arrow.

contains the contribution of secondary electrons brought about by inelastic scattering of photoelectrons. Thus it is not necessarily proportional to the number of generated primary photoelectrons, which is proportional to the absorption coefficient. However, in the spectrum measured up to $h\nu = 160$ eV, a very broad and intense band is found above $h\nu = 110$ eV. We ascribe this band to electrons suffering inelastic scattering and concomitant electrons excited by scattering. We take the total yield spectrum observed here below 100 eV to be proportional to the absorption spectrum.

In figure 9, weak peaks are found at $h\nu = 54$, 63, and 81 eV. They are denoted with vertical bars. The intensity rises steeply at the threshold of the 3p excitation at $h\nu = 66.2$ eV. The location is indicated with an arrow. Except for a weak feature located at $h\nu = 81$ eV, the total yield spectrum above the 3p threshold has roughly flat structure. This is quite contrasted with the CIS spectrum for the generation of the two-hole bound state shown in figure 5.

4. Discussion and conclusions

The experimental data presented in the preceding section raise two important issues. One is the profile of the MVV sCK spectrum. The other is how it is changed by the change in excitation energy. We summarize the results on the first issue as follows.

(1) The MVV sCK band of Ni has very low intensity. Thus the relaxation processes of the 3p hole include the prominent competing processes such as fluorescence.
(2) Four features are found in the MVV sCK band. In the excitation-energy range investigated in the present work, the lowest-kinetic-energy feature located at $\varepsilon_k = 49.8$ eV is separated from other features and has an FWHM of 1.7 eV. The width is caused by the lifetime of the state and phonons.
(3) The profile of the MVV sCK band excited with Mg Kα radiation does not coincide well with that excited with photons with energy below $h\nu = 110$ eV. Disagreement is distinct

as to the relative ratio of the intensity of component features; the feature at $\varepsilon_k = 49.8$ eV is not well separated from other features in EDC measured with the Mg Kα excitation.

(4) The profile of the MVV sCK band does not coincide with that of the LVV CK band. In particular, the MVV sCK band does not have a shape similar to that of the LVV CK band in which the features are ascribable to the multiplet structure arising from the atomic d^8 configuration. If the MVV sCK band is ascribable to the spectrum of the atomic d^8 configuration, both LVV CK and MVV sCK bands should give a similar profile. Another possibility is that the transition moments of the component lines of the multiplet arising from the d^8 configuration are considerably different between the CK and sCK transitions. However, this assumption does not explain the difference in the locations of the component lines. The MVV sCK spectrum of metallic Ni has a profile completely different from that of the MVV sCK spectrum of an isolated Ni atom that can be interpreted in terms of the multiplet coupling and the configuration interaction [22, 23].

The results summarized above appear to indicate that the final state generating the MVV sCK spectrum of Ni excited with light cannot be interpreted in terms of the quasi-atomic energy levels. Rather, we consider that indispensable magnitude of the energy band effect is involved in the transition process. According to the Cini–Sawatzky theory [31–33] the profile of the Auger band becomes the self-convoluted band of the valence band in the limit of the low intra-atomic Coulomb energy. Let us consider a simple picture. Suppose the valence band is composed of two rectangular-shaped bands with the same width, W, separated by energy distance d; the ratio of the heights is assumed to be $1{:}h$. The self-convoluted band comprises three component bands of the triangular shape with the same half width of W separated by the same distance, d; the ratio of the heights of the component bands is $1{:}(1/h + h){:}1$. Suppose that $h = 0.2$ and $d = 6.0$ eV as is the case of the main 3d band and the two-hole-bound-state band. Then the intensity ratio must be 1:5.2:1. If we assume that the features at $\varepsilon_k = 59.5$ and 60.5 eV are inseparable, the observed ratio is 1:1.25:0.038. The component separations are 6.5 and 3.2 eV. Any other shapes of the 3d band cannot explain the observed MVV sCK band reasonably through the self-convolution. Thus, we conclude that the simple self-convoluted-band picture cannot be applied. This point will be discussed later regarding the cause of the weak and narrow band at $\varepsilon_k = 49.8$ eV.

In this way, the two extreme pictures given in the Cini–Sawatzky theory [31–33] are not applicable to the MVV sCK spectrum of Ni. The spectrum should be taken for expressing the intermediate case where the intra-atomic Coulomb energy between two 3d holes, U, is not very different from the width of the 3d band, W. We consider that the final state of the MVV sCK transition is composed of the self-convoluted valence band deformed considerably by the intra-atomic Coulomb interaction between two 3d holes. If the valence band consists of a single component, the final-state band has two features. If the valence band consists of two component bands, the self-convoluted band has three component bands. Each of them has two component features. Then the MVV sCK band can have six component features at maximum. In practice, the component features overlap each other and the lifetime broadening obscures the structures. However, the assumption that the valence band has two component bands as we have made above leads to the situation that one of the components is the two-hole bound state. However there is no positive reason why an assumption like this is correct.

In the Cini–Sawatzky theory [31, 32], there is a case where both the split-off quasi-atomic line and the deformed self-convoluted band coexist. Thus, we can interpret the weak and narrow line at $\varepsilon_k = 49.8$ eV as being the split-off quasi-atomic line. If we consider that the separation between the centre of the intense components and the band at $\varepsilon_k = 49.8$ eV gives the rough value of effective U, we can evaluate it as 8 eV. On the other hand, W is about

3 eV. The value of U of 8 eV appears to be too large if we compare the present spectrum with the numerically calculated model spectra given by Sawatzky and Lenselink [32]. We do not find any multiplet components of the 49.8 eV line. The weak intensity of this band makes it difficult to find such a fine structure.

The Cini–Sawatzky theory [31, 32] does not seem to explain the observed MVV sCK spectra quantitatively. This theory is applicable to filled bands like the 3d band of Cu. We expect a filled 3d band in the intermediate state in Ni either in the low-energy-excitation case or in the case of considerable screening by conduction electrons.

Next we consider the fact that the profile of the MVV sCK band obtained by the Mg Kα excitation does not coincide with that excited with light in the region around $h\nu = 100$ eV. With Mg Kα radiation ($h\nu = 1253.6$ eV), electrons in the L_1 (2s, $\varepsilon_b = 1008.6$ eV), L_2 ($2p_{1/2}$, $\varepsilon_b = 870.0$ eV), L_3 ($2p_{3/2}$, $\varepsilon_b = 852.7$ eV), M_1 (3s, $\varepsilon_b = 110.8$ eV), M_2 ($3p_{1/2}$, $\varepsilon_b = 68.0$ eV), and M_3 ($3p_{3/2}$, $\varepsilon_b = 66.2$ eV) are excited. Then, transitions to extinguish a 2s hole, 2p holes, a 3s hole, and 3p holes occur following the pertinent core excitation. All these processes can generate 3p holes. Thus the MVV sCK transition occurs through several different de-excitation channels. Thus, the MVV sCK spectrum in the case of the Mg Kα excitation is complex and the widths of the component features are possibly increased. In LVV CK spectrum measurements, the widths of the bands can be decreased by coincidence spectroscopy [42].

The second issue is the change in the profile of the MVV sCK band caused by the change in excitation energy. The observed results are summarized as follows.

(5) The profile is changed at $h\nu = 78$ eV. The changed profile is recognized in the region below this energy, i.e. $h\nu \leqslant 78$ eV.
(6) For excitation energy above $h\nu = 66$ eV, the width of the two-hole-bound-state band is enhanced as excitation energy is increased.
(7) For the excitation-energy region $76 \geqslant h\nu \geqslant 71$ eV, the MVV sCK spectrum overlaps the two-hole-bound-state band and is deformed appreciably. Both bands are inseparable.
(8) In the range $76 \geqslant h\nu \geqslant 67$ eV, the location of the highest peak, the apparent peak of the two-hole-bound-state band, deviates from the constant-binding-energy line for $\varepsilon_b = 6.3$ eV.
(9) The complete merger of the MVV sCK band and two-hole-bound-state band occurs in the region $70 \geqslant h\nu \geqslant 66$ eV.
(10) The change in the profile of the MVV sCK band cannot be interpreted in terms of the intensity changes of the satellites at $\varepsilon_b = 11$ and 13.5 eV caused by resonance.
(11) The CIS spectrum for the two-hole-bound-state band exhibits the 3p–3d resonance in the region $80 \geqslant h\nu \geqslant 65$ eV. This covers an energy interval of 15 eV.
(12) The main 3d band shows the weak 3p–3d resonance.

In order to understand the observed results summarized above, we consider the outer-shell electronic states of Ni on the basis of the energy band picture. The energy bands are formed by the localized and correlated states with the d symmetry and widely spread conduction states with the sd symmetry. The band with d symmetry, referred to as the 3d band, is considerably affected by the electron correlation. In the practical calculation, rigorous formalism must be adopted [3, 4, 52].

According to the solid state data, the number of 3d electrons in a Ni atom is 9.4 on average [53]. Oh *et al* [54] pointed out that the distribution of the $3d^n$ configuration to give the average number of 3d electrons per atom is given by the binomial distribution if the correlation interaction between 3d electrons is ignored. The binomial distribution gives fractions of $3d^n$ to be 0.583, 0.344, and 0.088 for $3d^{10}$, $3d^9$, and $3d^8$, respectively. If this is correct, the major

component of the ground state of Ni arises from the d^{10} configuration. However, this is not the case. Jo and Sawatzky [55] claimed that the distribution of the 3d configurations in the ground state is 15–20% $3d^{10}$, 60–70% $3d^9$, and 15-20% $3d^8$ to explain the experimental data well. Tanaka and Jo [56] claimed that the distribution is 21%, 61%, and 18% for $n = 10$, 9, and 8, respectively. This gives the average number of 3d electrons per atom as 8.97. Tjeng *et al* [37] gave the distribution as $n = 16\%$, 49%, and 35%. The average number of 3d electrons per atom in their case is 9.19.

According to the reported results of the energy band calculation [52], the conduction band with large dispersion occurs in the region of binding energy larger than 4 eV. In this band, the mixing of the state with the d symmetry is weak. The majority of the 3d band exists in the binding-energy region below $\varepsilon_b = 3$ eV. At $\varepsilon_b = 1$ eV the 3d band exists with very small dispersion. In the region between $\varepsilon_b = 1$ and 3 eV, the bands with definite dispersion occur. They are 3d bands with the sd hybridization.

Even in the energy band state, the correlation interaction is important. It was shown [57] that the intra-atomic Coulomb energy governing an optical spectrum is a renormalized quantity and depends on the excitation energy. Qualitatively, this can be a part of the source of the dependence of the profile of the MVV sCK spectrum on the excitation photon energy.

The possible MVV sCK final states shown in figure 2 are reached from the intermediate state exhibited in figure 10. In the initial state, the 3d band designated as $V(h)$ with a hole at the Fermi level exists together with the conduction band arising from 4s electrons. Excitation light raises a 3p core electron far above the Fermi level. The resulting state with 3p core hole and a 3d hole forms the final state for the XPS 3p core line. However, this state has a very short lifetime. The strong attractive force caused by the inner-shell hole, $p(h)$, attracts conduction electrons, which remove the 3d hole at the Fermi level through screening. Thus, the intermediate state produced by the photoexcitation of the core electron consists of the filled 3d band and the core level state. The following Auger transitions lead to the different two-hole states shown in figure 2 according to the energy of the excited electron.

The Auger effect like the MVV sCK transition is caused by the localized transition involving a core hole. If the outer-shell state is the band state, two holes brought about by the transition may have different wavevectors $\mathbf{k}$ and $\mathbf{k}'$ and not necessarily be on the same lattice site. The Cini–Sawatzky theory [31, 32] employs an interesting approximation like the exciton state. It is similar to the method to make a Wannier exciton in a wide-gap semiconductor. There, the translational symmetry of electron energy and concomitant wavefunctions regarding the electron wavevector is utilized to introduce the configuration interaction. The translational symmetry regarding the space coordinate is also used. The configuration here stands for the arrangement of the wavefunctions in terms of the lattice site and the wavevector. By this approximation, the localized eigenfunctions are formed from the delocalized Bloch states. In this approximation, $\mathbf{K}_{ex}$ $(= \mathbf{k} - \mathbf{k}')$ has meaning.

A few final states are expected to occur according to the emergent intermediate states. This is the source of the excitation-energy dependence of the profile of the MVV sCK band. This issue will be treated later. The decay occurs quite fast. Thus the appreciable lifetime broadening is inevitable.

In general, the optically induced Auger transition including the sCK and CK transitions occurs to extinguish the core hole generated by the optical excitation. The electron jumping into the core level is in the relaxed outer-shell level. The MVV sCK transition in the present case, however, is not like this. The 3p photoelectron lines are found to be wide with FWHM reaching 5 eV. This suggests that the decay of the 3p hole occurs very fast. Naturally the sCK decay occurs while the 3p hole is being generated. Therefore, the optical excitation and the MVV sCK transition take place almost as a single process, not as the two-step process

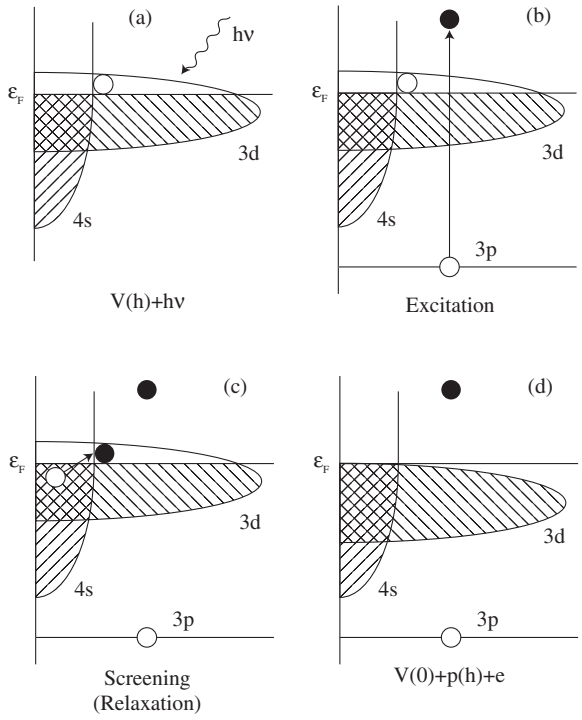

Figure 10. Generation of the intermediate state, $V(0) + p(h) + \mathrm{e}$. Black dots represent electrons, white circles holes, and ε_F the Fermi level. (a) Initial state with a 3d hole at the Fermi level, $V(h)$, and an incoming photon, $h\nu$. (b) Optical excitation of a 3p electron accompanied by the excitation of the 3d hole at the Fermi level by recombination (screening) with a conduction electron. (c) Screening of the 3d hole. (d) Optically generated intermediate state with the filled 3d band, $V(0)$, and the 3p level with a hole, $p(h)$.

where the optical transition occurs first and the sCK transition follows after the excited state is relaxed. The screening by conduction electrons also participates in the transition process.

We consider three possible final states illustrated in figure 2. The excitation-energy dependence of their generation is grouped as follows: (i) The case where $h\nu$ is sufficiently high. (ii) The case where $h\nu$ takes an intermediate magnitude. (iii) The case where $h\nu$ is low. The three cases are illustrated in figure 2 and summarized in table 1. In the final state configuration shown in table 1, the terms at the top give the major contribution. The other two terms give spectral deformation. The content of table 1 is explained below.

4.1. The case of sufficiently high excitation energy

When excitation energy is sufficiently high, the excited electron in the intermediate state illustrated in figure 10 is raised to a very high energy state. The excited electron does not interact with electrons in the valence band. Thus, the MVV sCK transition simply leads to a two-hole final state, $V(h + h)$. This state is not stable and its lifetime is short as mentioned already.

4.2. Intermediate-excitation-energy case

In this case, we consider that the optically excited electron interacts with two holes in the 3d band. The two-hole state with a screening conduction electron, which is the excited electron,

Table 1. Relations between the MVV sCK spectrum and the excitation photon energy. $V(h+h)$, valence band with two 3d holes; $V(h+h)+\mathrm{e}$, quasi-two-hole-bound state; $V(h^2)+\mathrm{e}^*$, two-hole bound state (see figure 2).

Excitation region	High energy	Intermediate energy	Low energy
$h\nu$	$h\nu \geqslant 79$ eV	79 eV $\geqslant h\nu \geqslant$ 71 eV $V(h+h)+\mathrm{e}$	71 eV $\geqslant h\nu \geqslant$ 66 eV $V(h^2)+\mathrm{e}^*$
Final state	$V(h+h)$	$V(h^2)+\mathrm{e}^*$ $V(h)$	$V(h+h)+\mathrm{e}$ $V(h)$
Resonant aspect	Non-resonant	Weakly resonant	Resonant
Name	sCK final state	Quasi-two-hole-bound state and single 3d hole state	Two-hole bound state and single 3d hole state
Remark	Unstable final state; large lifetime broadening	Mixture of the two-hole bound state and the sCK final state; complex spectral shape	Peak shift; broadened band

is generated. This state is shown in figure 2 as $V(h+h)+\mathrm{e}$ and referred to as the quasi-two-hole-bound state. The two-hole bound state, $V(h^2)+\mathrm{e}^*$, is also generated together with the main 3d band state, $V(h)$, with a 3d hole. Their intensities are not high.

The energy distribution of the quasi-two-hole-bound state in the first parenthesis in table 1 gives the major contribution to the observed spectra. The other two states deform the spectrum caused by the quasi-two-hole-bound state. The probability of generating the one-hole 3d band, $V(h)$, is considered to be small and the main part of the realized final state is $[V(h+h)+\mathrm{e}]+[V(h^2)+\mathrm{e}^*]$. However, the CIS spectrum for $\varepsilon_\mathrm{b}=0.6$ eV shows the weak resonance enhancement of the emission intensity above the threshold of the 3p excitation. This indicates the existence of the weak $V(h)$ final state.

In the intermediate-excitation-energy range, the MVV sCK spectrum has the profile that is given by the mixture of the quasi-two-hole-bound-state spectrum and the two-hole bound state. The profile is changed considerably with excitation energy. The details of this behaviour cannot be explained by the change in the intensity of the components of the multiplets of the $3d^8$ configuration. The final state with the quasi-two-hole-bound state gives the deformed MVV sCK spectra through the contribution of other two states. It has a form as if a conduction electron is trapped by the two 3d holes making a virtual bound state. If the screening is stronger, the two-hole bound state results. If the screening is far more complete, a single-hole state, $V(h)$, results, and it gives a state similar to the main 3d band. In the observed spectra presented in figures 6 and figure 7, the two-hole-bound-state peaks are conspicuous. However, it is possible that the major part of them is generated by the direct excitation of the valence band electron.

4.3. Low-excitation-energy case

The phenomena described here are related to the transition from the adiabatic to sudden approximation regimes as mentioned in section 1 [12]. We consider that the optically excited electron occupies the empty 3d level leading to the filled up 3d band even without the screening

by conduction electrons. Thus, the MVV sCK transition occurs in such a the manner that the two-hole bound state, $V(h^2) + e^*$, results. The existence of the quasi-two-hole-bound state, though weakly, slightly deforms the two-hole-bound-state spectrum. In other words, the different intermediate states with different energy reach different final states. That the main 3d state appears in the final state of the MVV sCK transition explains the weak resonance enhancement of the main 3d band above the 3p excitation threshold.

When the resonance occurs, the width of the two-hole-bound-state band is broadened. The peak shift is also recognized. As excitation energy increases, the features arising from the quasi-two-hole-bound state are split off as shown in figure 6.

In the generation of the MVV sCK transition, the role of the screening electron, the hybridized conduction electron, is important. The excited electron can occupy the state to form a well defined state, or it stays in the spectator-electron state according to its kinetic energy. This is similar to the case of the final state interaction referred to as the post-collision interaction describing the relation of atomic photoemission to the Auger effect [58]. Before the excited photoelectron leaves the atom, the Auger transition takes place and the excited photoelectron is affected by the potential of the two holes generated by the Auger transition. On the other hand, the Auger electron is affected by the potential screened by the optically excited electron, the spectator electron. Such interactions affect the kinetic energies of pertinent electrons. This phenomenon is distinct when the energy of the optically excited electron is low, since the spectator electron stays around the atomic core for a longer time. The post-collision–interaction phenomenon manifests itself as the shift of the Auger electron peak from the constant-kinetic-energy line toward high kinetic energy as excitation energy approaches the excitation threshold. A classical theory as well as a semiclassical theory was reported and investigators compared their data with both theories to find the qualitative agreement [58]. The relation between the kinetic-energy shift and the excitation energy is dependent on the lifetime broadening of the line [58].

As is obvious in figures 7 and 8, the deviation of the energy of the sCK electron from the constant-binding-energy line occurs toward the high-binding-energy side or the low-kinetic-energy side. This tendency is not necessarily against the cause of the energy shift found in the post-collision interaction in atomic spectra. The direct formation of the two-hole bound state does not totally participate in the 3p–3d resonance. In particular, the existence of the two-hole bound state that does not give resonance must be considered in detail. The phenomenon apparently means that the existence of two different final states having almost the same energy is seemingly against the results of simple quantum theory. In the case of the direct generation of the two-hole bound state, the photoelectron is affected by the potential of a 3d hole. In the case of the MVV sCK transition, the sCK electron is attracted by the potential of a 3p hole that is stronger. This makes the binding energy of the 3d electron higher and the kinetic energy of the emitted sCK electron lower.

Regarding the exciton-like state proposed in the Cini–Sawatzky theory [31, 32], the excited spectator electron can be trapped by the two holes generated by the sCK transition in the form of the virtual bound state, if the energy of the spectator electron is low. This is also a kind of final state interaction. If the energy of the excited electron is low, it is raised to the 3d state and participates directly in the sCK transition. Thus the form of the final state interaction is complicated. Theoretical investigations should be made on this issue.

An important fact is that the peak around $\varepsilon_b = 6.3$ eV is found in the whole excitation-energy region. The peak is clearly found in the region where the two-hole-bound-state band considerably overlaps the MVV sCK band and considerably destroys it. This indicates that the peak is attributed to the generation of the two-hole bound state by the direct excitation, as mentioned already. The direct formation of the two-hole bound state does not totally participate

in the 3p–3d resonance. Although the two final states could have different energy dependence, the two-hole-bound-state part resonates and the two final states cannot be distinguished. As mentioned already, the resonance takes place incompletely in some excitation-energy region. The kinetic energy of the emitted electron is affected by holes in the mixed states. This is a sort of final state interaction and shows up in the shift of the energy of the emitted electron.

In the case of metallic Ni, the phenomenon described above raises the problem of the investigation of the intermediate state and the final state in detail. This is especially interesting since the whole transition process must be treated as a single process. The issue has not been investigated theoretically. Igarashi *et al* [59] developed the theoretical treatment of the three-body interaction as applied to the resonance problem. The further development of the theory is invoked.

In the present study, the aspect of how two superficially different final states, the two-hole bound state and the MVV sCK final state, mix and become indistinguishable has been traced. This behaviour is seemingly similar to the Lu–Fano effect in atomic spectra [60].

The CIS spectrum gives the energy distribution of the state with constant binding energy from which photoelectrons are excited. The resonance-interference region of the two-hole bound state and the MVV sCK final state extends up to 20 eV above the Fermi level as found in figure 5. This range is much wider than the width of the empty 3d band found in the inverse photoemission data [51]. This wide range is brought about by the 3p–3d resonance. It is not the width of the localized state but the energy region of the continuous band that is responsible for the resonance-interference.

The difference between the LVV CK and MVV sCK spectra must be remarked. If we consider only the atomic final state with the configuration $3d^8 4s$, there is no difference between the final states of the LVV CK and MVV sCK transitions as pointed out already. In fact, figure 4 shows considerable difference. As described so far, we consider that the simple atom model is not applicable to the MVV sCK transitions. In the LVV CK transition, the large attractive potential of the 2p hole makes the outer-shell electron orbits shrink and the states of the outer-shell electrons become more like the atomic states. This is very different from the Doniach–Šunjić effect [19], in which conduction electrons are inelastically scattered by the 2p hole. The 2p hole does not only give rise to the Fermi-edge singularity but also alters the whole outer-shell electron state. This is evident in the occurrence of the white lines [38, 41, 44, 21, 46]. In the quasi-atomic sense, the nature of the screening electron changes as excitation energy changes. This change affects the effective intra-atomic Coulomb energy, U, and the intensities and the spectral distribution of multiplet lines. This may explain the observed difference among the LVV CK spectra, the MVV sCK spectra obtained by excitation with low energy photons, and the MVV sCK spectrum obtained by the Mg Kα excitation. In order to confirm this point for examining the applicability of the quasi-atomic model to the MVV sCK transition, it is useful to make the atomic multiplet calculation. However, we postpone this calculation and will present the calculated results in the near feature.

On the other hand, the absorption spectrum of the 3p electron known from the total yield spectrum shown in figure 9 exhibits a steep onset of absorption and a roughly flat band above it. This is more like the absorption to the unoccupied energy band. In the case of the CK transition, it is influenced by the potential of the core hole on the valence state. Even if a 2p hole is generated suddenly and the potential for the outer-shell electron changes abruptly, the overall optical transition follows successively in a finite time [61]. Even though the transition occurs as a single process, the change in the outer-shell state in the intermediate state definitely affects the observed spectrum.

Acknowledgments

The authors appreciate useful discussion with Professor T Fujiwara of the University of Tokyo. They also thank all the members of the technical staff of the National Synchrotron Research Center for their support.

References

[1] Guillot C, Ballu Y, Paigné J, Lecante J, Jain K P, Thiry P, Pinchaux R, Pétroff Y and Falicov L M 1977 *Phys. Rev. Lett.* **39** 1632
[2] Penn D R 1979 *Phys. Rev. Lett.* **42** 921
Liebsch A 1981 *Phys. Rev.* B **23** 5203
Kotani A and Toyozawa Y 1974 *J. Phys. Soc. Japan* **37** 912
[3] Davis L C and Feldkamp L A 1981 *Phys. Rev.* B **23** 6239
[4] Jo T, Kotani A, Parlebas J-C and Kanamori J 1983 *J. Phys. Soc. Japan* **52** 2581
[5] Girvin S M and Penn D R 1981 *J. Appl. Phys.* **52** 1650
Ohmura Y and Sato T 1990 *J. Phys. Soc. Japan* **59** 725
[6] Björneholm O, Andersen J N, Wigren C, Nilsson A, Nyholm R and Mårtensson N 1990 *Phys. Rev.* B **41** 10408
[7] Armen G B, Aksela H, Åberg T and Aksela S 2000 *J. Phys. B: At. Mol. Opt. Phys.* **33** R49
[8] Kleiman G G 1982 *Appl. Surf. Sci.* **11/12** 730
[9] de Siervo A, Landers R and Kleiman G G 2001 *Phys. Rev. Lett.* **86** 1362
[10] Grehk T M, Drude W, Treusch R and Materlik G 1998 *Phys. Rev.* B **57** 6422
[11] Drude W, Treusch R and Materlik G 1995 *Phys. Rev. Lett.* **74** 42
[12] Morais J, de Siervo A, Landers R, de Castro S G C and Kleiman G G 1999 *Surf. Sci.* **433–435** 878
[13] Sarma D D, Barman S R, Cimino R, Carbone C, Sen P, Roy A, Chainani A and Gudat W 1993 *Phys. Rev.* B **48** 6822
[14] Sorensen S L, Schaphorst S J, Whitfield S B, Crasemann B and Carr R 1991 *Phys. Rev.* A **44** 350
[15] Chiarello G, Amoddeo A, Agostino R G, Caputi L S and Colavita E 1993 *Phys. Rev.* B **48** 7779
[16] Himpsel F J, Eastman D E and Koch E E 1980 *Phys. Rev. Lett.* **44** 214
[17] Lund C P, Thurgate S M and Wedding A B 1994 *Phys. Rev.* B **49** 11352
[18] Kivimäki A, Aksela H, Aksela S and Sairanen O-P 1993 *Phys. Rev.* B **47** 4181
[19] Doniach S and Šunjić M 1970 *J. Phys. C: Solid State Phys.* **3** 285
[20] Föhlisch A, Karis O, Weinelt M, Hasselström J, Nilsson A and Mårtensson N 2002 *Phys. Rev. Lett.* **88** 027601
[21] Coulthard I, Sham T K, Hu Y-F, Naftel S J, Kim P-S and Freeland J W 2001 *Phys. Rev.* B **64** 115101
[22] Schmidt E, Schröder H, Sonntag B, Voss H and Wetzel H E 1984 *J. Phys. B: At. Mol. Phys.* **17** 707
[23] Tiedtke K, Gerth Ch, Kanngießer B, Obst B, Zimmermann P, Martins M and Tutay A 1999 *Phys. Rev.* A **60** 003008
[24] Songsiriritthigul P, Nakajima H, Wongkokua W, Kantee S, Kakizaki A, Pairsuwan W and Ishii T 2005 *Proc. 14th Int. Conf. on Vacuum Ultraviolet Radiation Physics (Cairns, 2004)* ed A Kheifets; *J. Electron Spectrosc. Relat. Phenom.* **144–147** 569
[25] Himpsel F J, Knapp J A and Eastman D E 1979 *Phys. Rev.* B **19** 2919
Eberhardt W and Plummer E W 1980 *Phys. Rev.* B **21** 3245
[26] Sakisaka Y, Komeda T, Onchi M, Kato H, Masuda S and Yagi K 1987 *Phys. Rev. Lett.* **58** 733
[27] Okane T, Kashiwakura T, Suzuki S, Sato S, Kinoshita T, Kakizaki A and Ishii T 1993 *Z. Phys.* B **91** 437
[28] Kashiwakura T, Suzuki S, Okane T, Sato S, Kinoshita T, Kakizaki A, Ishii T, Isikawa Y, Yamagami H and Hasegawa A 1993 *Phys. Rev.* B **47** 6885
[29] Clauberg R, Gudat W, Kisker E, Kuhlmann E and Rothberg G M 1981 *Phys. Rev. Lett.* **47** 1314
[30] Kinoshita T, Ikoma T, Kakizaki A, Ishii T, Fujii J, Fukutani H, Shimada K, Fujimori A, Okane T and Sato S 1993 *Phys. Rev.* B **47** R6787
[31] Cini M 1977 *Solid State Commun.* **24** 681
Cini M 1978 *Phys. Rev.* B **17** 2788
[32] Sawatzky G A 1977 *Phys. Rev. Lett.* **39** 504
Sawatzky G A and Lenselink A 1980 *Phys. Rev.* B **21** 1790
[33] Bennett P A, Fuggle J C, Hillebrecht F U, Lenselink A and Sawatzky G A 1983 *Phys. Rev.* B **27** 2194
[34] Jach T and Powell C J 1981 *Phys. Rev. Lett.* **46** 953
[35] Mårtensson N, Nyholm R and Johansson B 1984 *Phys. Rev.* B **30** R2245
[36] Cini M and D'Andrea A 1984 *Phys. Rev.* B **29** 6540

[37] Wegner T, Potthoff M and Nolting W 2000 *Phys. Rev.* B **61** 1386
[38] Tjeng L H, Chen C T, Rudolf P, Meigs G, van der Laan G and Thole B T 1993 *Phys. Rev.* B **48** 13378
[39] Anilturk O S and Koymen A R 2001 *J. Appl. Phys.* **89** 7233
[40] Weinelt M, Nilsson A, Magnuson M, Wiell T, Wassdahl N, Karis O, Föhlisch A, Mårtensson N, Stöhr J and Samant M 1997 *Phys. Rev. Lett.* **78** 967
Suga S, Kimura S, Matsushita T, Sekiyama A, Imada S, Mamiya K, Fujimori A, Takahashi H and Mori N 1999 *Phys. Rev.* B **60** 5049
[41] Magnuson M, Wassdahl N, Nilsson A, Föhlisch A, Nordgren J and Mårtensson N 1998 *Phys. Rev.* B **58** 3677
[42] Lund C P, Thurgate S M and Wedding A B 1997 *Phys. Rev.* B **55** 5455
[43] Ohno M 1998 *Phys. Rev.* B **58** 12795
[44] Iacobucci S, Sacchi M, Marassi L, Marocchi V and Stefani G 1999 *Phys. Rev.* B **59** 9898
[45] Petrov V N and Kamochkin A S 2004 *Rev. Sci. Instrum.* **75** 1274
[46] Knorren R, Bennemann K H, Burgermeister R and Aeschlimann M 2000 *Phys. Rev.* B **61** 9427
Pagliara S, Sangaletti L, Goldoni A, Kim C, Shen Z-X, Revcolevschi A, Dhalenne G and Parmigiani F 2002 *Phys. Rev.* B **65** 205107
[47] Songsiriritthigul P, Pairsuwan W, Ishii T and Kakizaki A 2003 *Nucl. Instrum. Methods Phys. Res.* B **199** 565
Songsiriritthigul P, Nakajima H, Kantee S, Wongkokua W, Pairsuwan P, Ishii T and Kakizaki A 2004 *Proc. 8th Int. Conf. on Synchrotron Radiation Instrument (San Francisco, 2003)* (*AIP CP* 705) ed T Warwick *et al* (New York: American Institute of Physics) p 372
[48] Wongkokua W, Nakajima H, Songsiriritthigul P, Pairsuwan W, Ishii T and Kakizaki A, unpublished
[49] Fuggle J C and Mårtensson N 1980 *J. Electron Spectrosc. Relat. Phenom.* **21** 275
[50] Fano U and Cooper J W 1968 *Rev. Mod. Phys.* **40** 441
[51] Tezuka Y, Kanai K, Ishii H, Shin S, Nozawa S, Tanaka A and Jo T 2004 *Phys. Rev.* B **70** 193107
Schedin F, Warburton D R, Thornton G and Hoyland M A 1998 *Phys. Rev.* B **57** 3491
[52] Weling F and Callaway J 1982 *Phys. Rev.* B **26** 710
[53] Kittel C 1971 *Introduction to Solid State Physics* 4th edn (New York: Wiley) p 538
[54] Oh S-J, Allen J W, Lindau I and Mikkelsen J C Jr 1982 *Phys. Rev.* B **26** 4845
[55] Jo T and Sawatzky G A 1991 *Phys. Rev.* B **43** R8771
[56] Tanaka A and Jo T 1992 *J. Phys. Soc. Japan* **61** 2669
[57] Yamasaki A and Fujiwara T 2003 *J. Phys. Soc. Japan* **72** 607
[58] Prideaux A and Madison D H 2003 *Phys. Rev.* A **67** 052710
Hanashiro H, Suzuki Y, Sasaki T, Mikuni A, Takayanagi T, Wakiya K, Suzuki H, Danjo A, Hino T and Ohtani S 1979 *J. Phys. B: At. Mol. Phys.* **12** L775
Schmidt V, Sandner N, Mehlhorn W, Adam M Y and Wuilleumier F 1977 *Phys. Rev. Lett.* **38** 63
[59] Igarashi J I, Unger P, Hirai K and Fulde P 1994 *Phys. Rev.* B **49** 16181
[60] Lu K T and Fano U 1970 *Phys. Rev.* A **2** 000081
Brown C M, Tilford S G and Ginter M L 1977 *J. Opt. Soc. Am.* **67** 584
[61] Schiff L I 1968 *Quantum Mechanics* 3rd edn (New York: McGraw-Hill) p 292